Fast Track

Sarah J. R. Staton[1]
Kang Ping Chen[2,3]
Thomas J. Taylor[4]
Jose Rafael Pacheco[4,5]
Mark A. Hayes[1]

[1]Department of Chemistry and Biochemistry and Center for Solid State Electronics Research, Arizona State University, Tempe, AZ, USA
[2]Department of Mechanical and Aerospace Engineering, Arizona State University, Tempe, AZ, USA
[3]College of Petroleum Engineering, China University of Petroleum, Beijing, P. R. China
[4]Department of Mathematics and Statistical Sciences, Arizona State University, Tempe, AZ, USA
[5]USA Environmental Fluid Dynamics Laboratories, Department of Civil Engineering and Geological Sciences, The University of Notre Dame, South Bend, IN, USA

Received August 30, 2010
Accepted September 1, 2010

Research Article

Characterization of particle capture in a sawtooth patterned insulating electrokinetic microfluidic device

Here we present a scheme to separate particles according to their characteristic physical properties, including size, charge, polarizability, deformability, surface charge mobility, dielectric features, and local capacitance. Separation is accomplished using a microdevice based on direct current insulator gradient dielectrophoresis that can isolate and concentrate multiple analytes simultaneously at different positions. The device is dependent upon dielectrophoretic and electrokinetic forces incorporating a global longitudinal direct current field as well as using shaped insulating features within the channel to induce local gradients. This design allows for the production of strong local field gradients along a global field causing particles to enter, initially transported through the channel by electrophoresis and electroosmosis (electrokinetics), and to be isolated *via* repulsive dielectrophoretic forces that are proportional to an exponent of the field gradient. Sulfate-capped polystyrene nano and microparticles (20, 200 nm, and 1 μm) were used as probes to demonstrate the influence of channel geometry and applied longitudinal field on separation behavior. These results are consistent with models using similar channel geometry and indicate that specific particulate species can be isolated within a distinct portion of the device, whereas concentrating particles by factors from 10^3 to 10^6.

Keywords:
Dielectrophoresis / Particle trapping / Separation

DOI 10.1002/elps.201000438

1 Introduction

In addition to traditional methods (*e.g.* size exclusion, filtration, centrifugation, *etc.*), the separation of particulates (100 nm to 10 microns) has employed either electrophoretic (EP) or dielectrophoretic (DEP) forces. In EP size and surface charge define the interactions, whereas the DEP force is influenced by all physical, electrostatic and electrodynamic properties of the particles and surrounding solution. As described by Pohl [1] in the 1950s, DEP utilizes non-uniform electric fields to take advantage of polarization and permeability of neutral bodies as well as the permeability of their surrounding medium to create separations. When applied to biological targets, these features allow subtle changes in biochemistry that effect cell polarizability to be exploited for separating bioanalytes, including discriminating living *versus* dead or various metabolic states [2–4]. The application of DEP extends far beyond bioseparations, ranging from simple statically charged amber to the ground breaking foundational work of Pohl which focused on the action of DEP on suspensions [5]. The DEP forces can be induced by both alternating current (AC) and direct current (DC) fields, and is used for environmental samples and blood-based diagnostics [6–12], along with viral isolation [13–15]. DEP-based systems have successfully separated, isolated, and manipulated particles from a few nanometers to approximately 100 μm, encompassing many targets of great interest [16].

Conventional applications of DEP are generally limited to the bifurcation of samples where one component of a mixture is retained, whereas others that flow through or mixtures are separated into two sub-populations. This is true in both the DC and AC regimes. Also, embedded

Correspondence: Professor Mark A. Hayes, Arizona State University, Department of Chemistry and Biochemistry, MS 1604, Tempe, AZ 85287, USA
E-mail: MHayes@asu.edu
Fax: +1-480-965-2747

Abbreviations: AC, alternating current**; DC,** direct current**; DC-iGDEP,** direct current insulator gradient dielectrophoresis**; DEP,** dielectrophoresis**; EP,** electrophoretic **iDEP,** insulator dielectrophoresis **IGS,** insulating gradient structure

electrodes are often used, leading to several negative impacts on separations; including undesirable chemical reactions at the electrode surface and gas formation due to electrolysis of the surrounding fluid. Some of these effects are minimized by using AC fields; however, using solely AC fields prevents the use EP forces for separation.

The separative advantage of DEP and EP in comparison to more traditional techniques such as standard filtration and ultracentrifugation is the richness of the vectors of separation inherent to DEP and EP. Where both filtration and ultracentrifugation depend on the size and mass of the analyte, DEP and EP can fine tune multiple physical property vectors. As a result DEP and EP are capable of yielding a higher resolution separation.

This work builds on the insulator-based DEP (iDEP) work of Cummings and Singh [17]. This technique utilizes insulating material to shape the electric field, and allows the electrodes to be placed at a distance from the area of the separation [4, 17–23]. Moving the electrodes away from the separation zone minimizes the impact of reactions and gas production. With these problems mitigated, DC fields can be used so that both EP and DEP forces can be simultaneously exploited. Whereas early iDEP designs depended on insulating features in parallel that obstruct the channel, in this work the insulator structures are placed at the edge of the channel (Fig. 1) to shape gradients and allow multiple distinct traps of differing strength along the length of the device. This combination of global channel taper and non-uniform field gradients produces a design that utilizes both EP and DEP forces in opposition as modeled in Chen *et al.* [24]. The use of both EP and DEP allows size, charge, polarizability, deformability, surface charge mobility, dielectric features, and local capacitance to be exploited for the separation and the resolution of the analytes.

The direct current insulator gradient dielectrophoresis (DC-iGDEP) strategy has proven very useful for the separation of several species live/dead bacteria [4]. While this proved its utility, the DEP forces are extremely difficult to quantify because of the complexity of the physical properties of the bacteria. In contrast, this work examines the behaviors of well-described polystyrene particles in a DC-iGDEP system to better understand the underlying forces. Further, the range of influence is established across a wider range of the analyte sizes (20, 200 nm, and 1 μm) mimicking bioanalytes from viruses to cells. Upon introduction to the more open end of the channel, particle movement is dominated by EP and EOF. Once the particles enter the saw tooth patterned portion of the channel described further as the insulating gradient structure (IGS), particle motion combines EP and EOF with a countering DEP force. The balance of these forces and their action on the various physical properties of the analytes enable device to act as an amalgamation of single separation processes. Selective capture and resolution of polystyrene particles are shown over the range of 20 nm–1 μm individually as well as some co-capture of two different sizes using DC-iGDEP.

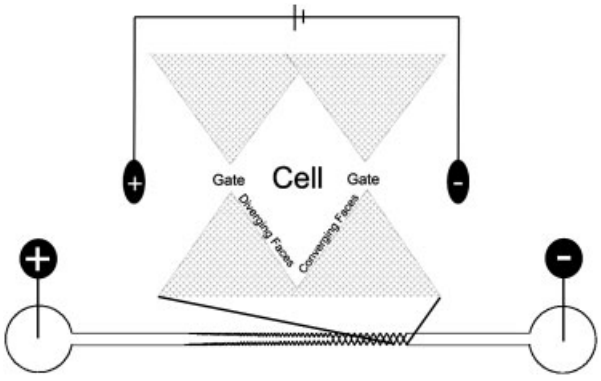

Figure 1. Diagram of the basic unit of the IGS including the vocabulary to discuss particle position within the structure. A schematic of the total device that is made from several repeats of different sized basic units is given. The IGS is connected with straight walled channels to reservoirs used for sample introduction and electrode placement.

2 Materials and methods

2.1 Fluorescent particles

Sulfate-capped fluorescent green polystyrene particles of 20, 200 nm, and 1 μm diameter with 505/515 excitation/emission properties were used as well as 1 μm red polystyrene particles with 580/605 excitation/emission (Invitrogen, Carlsbad, CA, USA). Particles were suspended in a circumneutral 2 mM phosphate buffer. A portion of the particle solution was introduced into the channel *via* the reservoir at the broader end of the device (Fig. 1).

2.2 Device fabrication

The microfluidic devices were fabricated using standard photolithography, fabrication, and bonding techniques [25]. Devices were cast using Sylgard 184 silicone elastomer kit PDMS (Dow/Corning, Midland, MI USA). The photomasks were designed using AutoCAD (Autodesk, San Rafael, CA, USA) and photolithographic positive stamps were made using AZ P4620 photoresist (AZ Electronic Materials, Branchburg, NJ, USA) and contrast enhancement material CEM388SS (Shin-Etsu MicroSi, Phoenix, AZ, USA). Devices were fabricated from PDMS with a glass cover plate (Home Depot door glass replacement squares, Tempe, AZ, USA). The glass cover plates were triple washed with alconox, 18 MΩ water, and isopropyl alcohol. After which they were baked overnight at 450°C. Shortly after the PDMS portion of the device was fabricated, access holes were made using a hole punch, 3 mm diameter through 0.5–1 cm of PDMS, and then was sealed to a glass cover plate by plasma oxidation, followed by contact sealing [26]. For some devices, the only one, or the other, surface was treated with the plasma.

The geometry of the IGS consisted of successive triangular units that extended into the open volume to induce

local electric field gradients. The insulating PDMS 60° triangles begin with a base length of 6 μm and a height of 5.2 μm. Their side length and width increase by 40 μm after every six repeats (Fig. 1), resulting in an initial gap distance is 945 μm and the final gap distance being 27 μm. The IGS connects the two reservoirs created by the hole punch, where sample and buffer were introduced to the channel. The channel depth ranged from 13 to 16 μm.

2.3 Experimental settings

Sample was introduced *via* the reservoir at the end of the IGS with the larger gap distance. After sample introduction, platinum wire electrodes (0.404 mm external diameter 99.9% purity, Alfa Aesar, Ward Hill, MA, USA) were placed in each of the reservoirs in contact with the solution and attached to a power supply (Series 225, Bertram). The voltage was set at the specified potential, between 50 and 1200 V, for the time specified, between a few seconds and several hours for each experiment.

Visualization was achieved using an Olympus inverted IX70 microscope with a mercury short arc H30 103 w/2 light source from OSRAM and an Olympus DAPI, FITC, Texas Red triple band pass cube (Olympus, Center Valley, PA, USA). Images of the device were captured using a miniVID video camera (LW Scientific, Lawrenceville, GA, USA) that saved color.avi formatted files.

2.4 Image processing

Images of the IGS as single still frames were taken from the raw date file (stored in the .avi format) using Microsoft Windows Movie Maker. From these still frames, images of each cell (Fig. 1) along the channel were stored as individual images. These images were used to construct mosaics of the entire channel as well as used in Mathematica to quantitate the red, green, and blue channels of the image. The data presented represent multiple replicates ($n > 3$) with isolation events occurring in the same position.

3 Results

Polystyrene particles were used as probes of the electrokinetic and DEP behaviors of the device. Isolation and concentration of sulfate-capped 20, 200 nm, and 1 μm (two types, red and green) diameter particles were demonstrated under a variety of conditions.

Two terms are defined here to facilitate discussion. Gate is defined as the area directly between the narrowest portions of local IGS immediately between the teeth points, defined by the insulating wall material. A cell is defined as the volume between and within two gates (Fig. 1). Further, the diverging (increasing channel width) and converging (decreasing width) faces are also defined. The designation of diverging and converging is given relative to the direction of the EP movement of a positively charged particle. This unit is repeated several times within the complete device with varying physical dimensions. Within the cell, the local field gradient is defined by the diverging and converging faces of the insulating wall of the IGS in response to the global applied field.

Surface treatment variations resulted in slightly differing behaviors of the probe particles. Plasma oxidation was used to convert the PDMS surface temporarily to hydrophilic silanol groups and allow bonding to the glass cover plate. By treating both the PDMS surface and glass cover plate, a non-reversible bond is created, whereas only treating the PDMS channel and then contact-sealing to the glass resulted in a reversible bond. Depending upon whether one or both surfaces were treated, characteristic behaviors were observed, described in detail below, which are attributable to variations in local EOF. By treating only the PDMS portion, the movement and the behavior of the particles within the IGS appeared more orderly, whereas when both surfaces are treated the movement appears to be more chaotic.

One set of experiments focused on the behaviors of a mixture of 200 nm and 1 μm diameter particles. Fluorescent micrographs (with some white light illumination to accent wall features) of the narrowest portion of the IGS containing 200 nm green spheres as well as 1 μm red and green spheres were captured (Fig. 2). The device had been prepared by plasma treating only the PDMS channel that was then contact-sealed to a glass cover plate producing a reversible bond. Matched images of the colloid dispersed throughout the IGS (Fig. 2, bottom), without an applied electric field, and with the field applied (Fig. 2, top) were compared. Observing the differences before and after the application of the external electric field demonstrated typical behavior for these particles within the IGS. Upon application of the field (150 V/cm, average global), the 200 nm green particles are forced immediately (<1 s) into discrete arcs on the converging face and establish a steady state after just 5 s. The arc occupied a volume of approximately 100 pL. These 200 nm particles are not visible as individual particles (below the optical diffraction limit) or at the initial concentration chosen for these experiments. They only become visible upon the isolation and concentration processes upon application of an external electric field. While the 200 nm green particles are collected in these arcs at the converging faces the 1 μm red and green particles were observed to stream quickly through the cells and gates in the opposite direction of the 200 nm particle capture. Effectively the 1 μm particles were separated and removed from the 200 nm particles.

The capacity for this technique to concentrate particles was investigated using the 200 nm particle data. In order to define and quantitate an enrichment factor or the amount of concentration increase of the analytes, several approaches were taken. First, the light intensity within the focused arc was compared to an area within the cell with no detected fluorescence (prior to application of potential). To compensate for the bright field illumination, the blue channel intensity was subtracted, since the particle fluorescence was

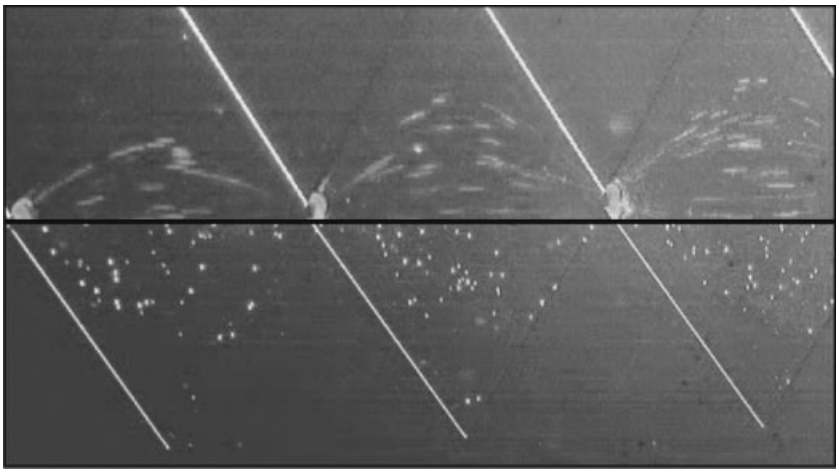

Figure 2. Side-by-side comparison separated by the middle black line of the device with and without an applied electric field. The channel contains 1 μm red and green particles in addition to 200 nm green particles. The top panel shows the channel and its contents exposed to 150 V/cm. Within 5 s capture of the 200 nm particles on the converging face near the gates small arcs were observed while the 1 μm particles stream through. The bottom panel shows the channel and all of the particles dispersed completely throughout the channel without voltage being applied. Note that the 200 nm green particles are not detectable in the absence of the applied electric field.

in the green channel only. From this spectroscopic approach an increase of $\sim 4 \times 10^3$ was determined at a single gate. Within the IGS there are six gates of the same gap distance. Assuming the same enrichment factor for each of those six gates the global device would have an enrichment factor of 2.4×10^4 times assuming identical capture along the six gates. Alternatively, this enrichment could also be viewed in terms of particles isolated. Using the volume of a 200 nm spherical particle, 2.4×10^4 particles could reside in the 100 pL capture volume. Extended to the six gates, $\sim 1.4 \times 10^5$ particles are isolated. Finally, the enrichment factor can be as high as 3×10^6 – given the entire particle load, meaning the device is not overloaded – in a sample volume of 50 μL was completely captured in a volume of 100 pL at the gates as observed in the experimental data.

The individual intensities of the red, green, and blue channels of the raw data file for each cell over the length of the IGS were used to assess the selectivity of processes (Fig. 3). The cell number is counted from the exit at the narrowest portion of the device (cell ♯1) toward the widest portion of the device. Cell number is counted from the narrowest end arbitrarily to minimize the cell number magnitude where isolation is achieved. Above the graph (Fig. 3) is a photo composite of the channel from which the red, green, and blue intensities were extracted using in-house developed Mathematica program. The background was established from the average of cell numbers 7–9 (black in the photo mosaic), where the resulting magnitude was subtracted from the rest of the cell values. The device was plasma treated only on the PDMS channel portion and was filled with 20 nm green particles and 1 μm red particles. The sample was exposed to 287 V/cm (average global field) for approximately 4 min. Isolation and concentration were observed *via* the increased signal response in the green channel, along with visual evidence, of only the 20 nm particles in the first and second cells of the device. The capture of the particles appears to be throughout the cell with slightly increased particle density toward the converging face of the cell.

Given a similar treatment, 1 μm green particles are shown to isolate and concentrate in a discrete zone found in cells 5 and 6 after 150 V/cm (average global) was applied (Fig. 4). The image was captured using both bright field illumination and fluorescence to aid in determining the geography of the particle capture along the IGS's length. The zone of particle isolation is clearly observable with the increased intensity found in cells 5 and 6 along with the bright spots visualized in the device mosaic above the plot. Especially when compared to the rest of the device's intensity where little to no fluorescence can be observed indicating the ability of the device to concentrate and localize the analyte. The captured particles are on the converging face of the cell. The background was averaged and used for subtraction using the intensity from cells 1, 2, and 9–25.

Treating both the PDMS channel as well as the glass cover plate with the plasma created a non-reversibly bonded device that was able to simultaneously capture 200 nm green particles in one zone while capturing 1 μm red and green particles in a different zone (Fig. 5). The background was taken as the average of cells 1 and 3. The channel was exposed to 150 V/cm (global average) to elicit capture. Although the channel was greatly overloaded with particles as evident from the bright spots of non-specific absorption, these zones were distinguishable from the areas of field controlled capture by noting particle relaxation after the voltage was removed. If no relaxation was observed then the spots were masked (effectively subtracted) during the intensity determination. Capture of the 200 nm green particles in cell 2 as well as capture of most of the 1 μm particles both red and green were observed at cells 11 and higher. The 200 nm particles appear to have been captured both at the converging face and throughout the upper portion of cell 2. While the 1 μm particles were observed at the converging faces of the cells where they were captured.

4 Discussion

Expanding current understanding of the abilities of DC-iGDEP to isolate particles over a biologically relevant range of particle sizes was accomplished using fluorescent

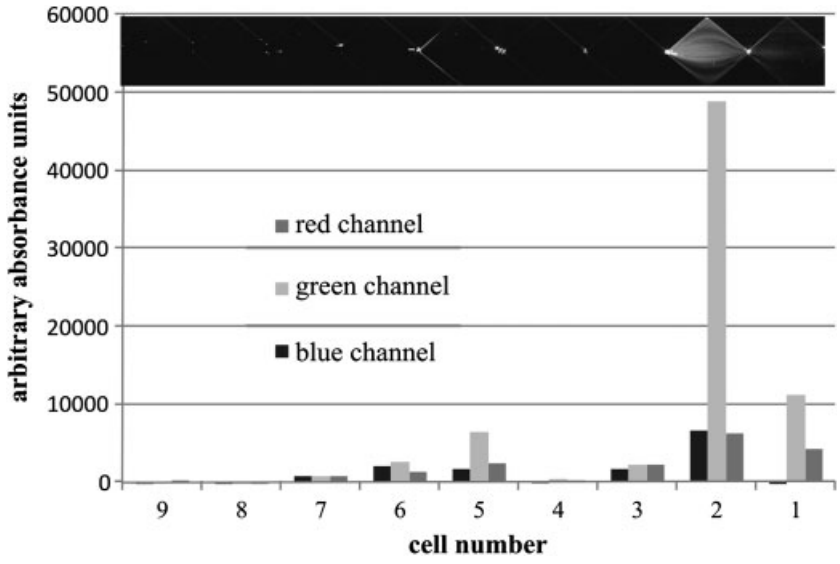

Figure 3. Graph of the intensity of the red, green, and blue channel intensity axially along the IGS. The device contained 1 μm red and 20 nm green particles exposed to 287 V/cm. Cell number is counted from the narrow end of the IGS to the broadest portion. Clear capture of the 20 nm green particles was observed in cell numbers 1 and 2 as can be seen in the photo mosaic of the IGS in the upper portion of the graph.

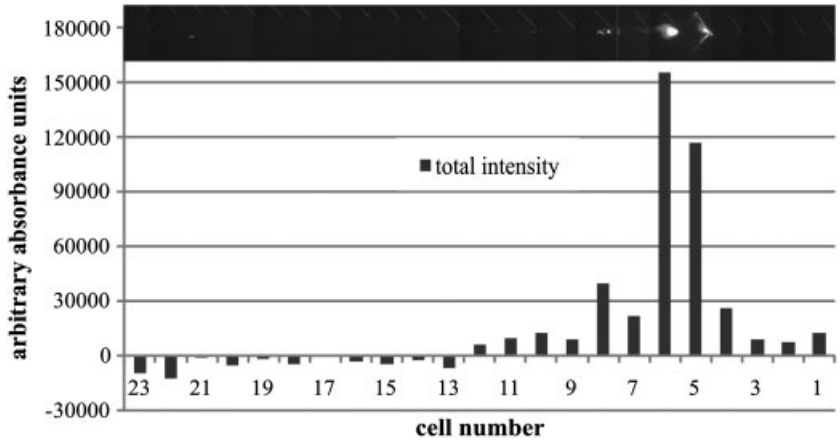

Figure 4. Total intensity of the red, green, and blue channel intensities combined graphed along the IGS. The channel contained 1 μm green particles exposed to 150 V/cm. Clear capture of the 1 μm green particles was observed in cell numbers 5 and 6 observable as bright spots in those cells in the above mosaic.

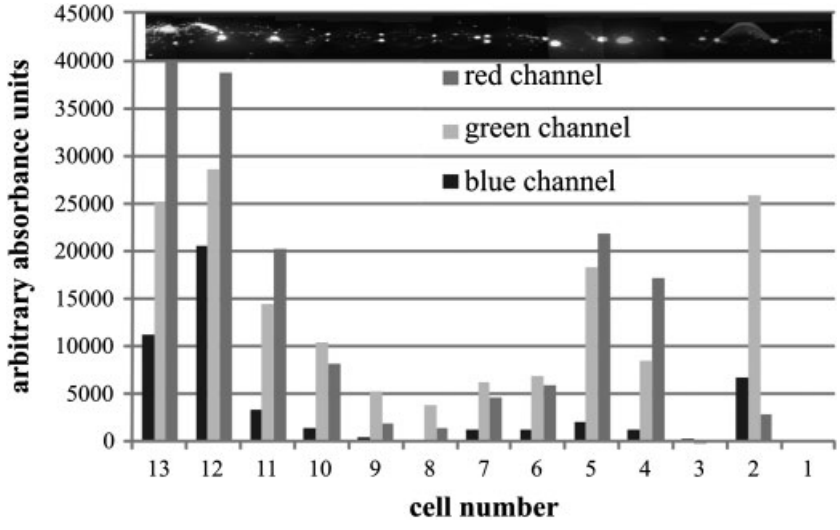

Figure 5. Graph of a section of the IGS containing 1 μm red and green particles along with 200 nm green particles exposed to 150 V/cm divided into the total intensity of the red, green, and blue channel intensities. Clear capture of the 200 nm green particles was observed in cell number 2 with capture of 1 μm particles up field of cell 11, specifically in cells 12 and 13 as seen in the mosaic of the IGS. Some particle overloading was observed in the form of nonspecific absorbed spots of particles further explored in the Section 3.

polystyrene particles with well-defined physical properties. In this study, the particle size ranged from 20 nm to 1 μm, consistent with several biologically and biomedically relevant bioanalytes (Fig. 6). For instance, several different types of bacteria range in size from 1 to 10 μm [27] with some common water-borne pathogenic bacteria *Cryptosporidium parvum* and *Giardia intestinalis* being ~5 and ~10 μm, respectively [28]. These bacteria are known to be common sources of infection from untreated or improperly treated water in both the underdeveloped and industrialized world [29]. This size range overlaps the current work as well as the previous bacterial separations of Pysher and Hayes [4]. Viruses generally range in the size from several tens of nanometers to roughly 100 nm [27]. This includes common viruses like the influenza virus strain H1N1 (120 nm) [30, 31] or the lethal human immunodeficiency virus (120 nm) [32]. These potential future targets fit well within the size range of the particles tested and may point to new application for this technology. The benefits of DC-iGDEP technology over current methods for these applications would be its ability to capture multiple analytes along the length of the device, its open channel design (compared to filter approaches), and its speed of separation. The co-capture of several bioanalytical targets could allow for simultaneous testing as well as separate purification within a single step process. In combination with the open channel design in IGS could allow for in-channel detection elements or for the system to be pressurized for further off-line analysis without further preparative steps to remove interfering sample matrix, like gels, or culturing media that could hamper testing. Finally, the ability for DC-iGDEP to quickly separate targets in the order of tens of seconds to a few minutes exceeds current technology used for these applications. Therefore, this work displays great promise by manipulating particles in this size range for future applications expanding for several bioanalytes: viruses, organelles, bacteria, and animal cells.

The capability to manipulate 200 nm particles quickly and economically would prove to be a serious breakthrough for several different industries working with analytes from a few nanometers to 100 μm [16]. As shown in Fig. 2, 200 nm particles were discretely concentrated in several bright arcs, each 100 pL. The particles were shown to collect after only 5 s of applied field. However, not only were the 200 nm green particles shown to selectively capture, but 1 μm green

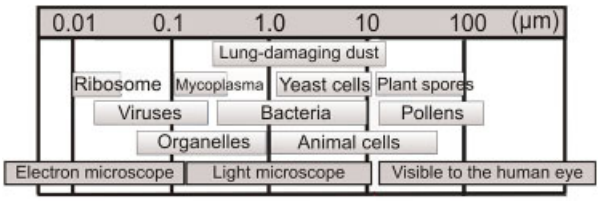

Figure 6. Size range of common bioanalytes compared to the necessary methods of visualization. Adapted from www.invitrogen.com.

and red particles were free to stream through the device toward the reservoirs where they could be collected or removed. Current methods like laser light scattering can be used to analyze size distribution in complex sample, but to be able to physically separate the current methods generally employed are filtration, gradient ultracentrifugation, and size exclusion chromatography [33]. The time necessary for filtration which is currently the fastest method takes a few seconds, but it only bifurcates the sample around a single size cut-off and needs larger samples. Size exclusion chromatography is more time intensive (tens of minutes or longer), but does physically separate analytes from a few nanometers up to several hundred nanometers [33]. The dynamic size range for size exclusion chromatography is slightly smaller than DC-iGDEP, the separation is also only based on size limiting the resolving ability of the technique. Other methods utilizing DEP for the bifurcation of samples do work more quickly. Yet, these methods depend solely on DEP and are subjected to the limitations of purely DEP forces detailed in the introduction, specifically the inability to exploit EP and its ability to separate based on size and surface charge.

In addition to the ease of isolation, the time of separation is also an important factor when hoping to mate a separative preparation system to either direct detection or further processing off-line in order to maintain bioanalyte viability. For these reasons the ability to maintain the viability of the bioanalyte is highly desirable. Although there has not been extensive amounts of research looking at the effects of separation on the viability of different bioanalytes, Gupta *et al.* have shown that both yeast and fibroblasts are able to withstand field strengths from 150 to 170 V/cm for approximately 45 min [34]. These field strengths are consistent with the global field strengths used in this study where the exposure times were lower, from 5 s to 20 min. It stands to reason that minimizing the time of exposure would be preferable in order to minimize the disturbance the cell sustains. Therefore, there is a high probability that this method could maintain bioanalyte viability allowing for further analysis.

To be able to evaluate the effectiveness of DC-iGDEP in comparison with other separation schemes some measure of resolution must be determined. One metric of the method's resolution is compared to the DEP size limit. This size limit is created when the thermal mixing forces (Brownian motion) exceeds the ability of the DEP force to separate and isolate. The force associated with Brownian motion increases as particle size is reduced making it more difficult to use DEP to manipulate smaller target bioanalytes. As treated by Pohl [1] the DEP lower size limit ranges lies from 10 to 100 nm. Using Pohl's approach DC-iGDEP is capable of overcoming the 2.07×10^{-12} N *per* particle forces in order to be able to capture and isolate the 20 nm polystyrene particles. The 20 nm particles captured here lie toward the lower end of the size limit range. This size of particle manipulation has been found in other types of iDEP [19, 21, 23] making DC-iGDEP

comparable to these methods. However, DC-iGDEP also allows for the exploitation of EP forces and separation as well as repeated multiple traps leading to the advantages of not being limited to bifurcation of the sample (co-capture) and higher capture yields than single trap systems like Clarke or Calander [21, 23].

Building upon this work along with the theoretical work of Chen *et al.* [24] and the bacterial separations of Pysher and Hayes [4] the direction of predictive design of DC-iGDEP for specific bioanalytes could be achieved through the control of several tunable parameters. In addition to the experimental conditions of varying voltage and buffer composition and strength, there are several device design conditions that could be tailored to particular bioanalyte. The electrical field can be shaped and manipulated by changing the shape, dimensions, and spacing of the insulating features. These parameters influence not only the shape of the electric field, but also change the electric field gradient on which DEP depends. Different materials, varying plasma treatments, and surface coatings can also be used to alter properties like EOF [35]. By understanding the EP and DEP mobilities of target bioanalytes combined with the theoretical model of Chen *et al.*, these different fabrication and experimental conditions can be manipulated to fit the necessary conditions.

Several lines of evidence presented here display promise for the separation of complex mixtures and the tunable nature of the DC-iGDEP. Given the diverse targets already tested from biologically (bacteria) to variously sized polystyrene particles (20 nm–1 μm) DC-iGDEP may have applications is several settings where target analytes are low in concentration. For example, environmental applications could include waste water monitoring for harmful bacteria where small colonies are greatly diluted in large volumes of liquid. Biomedical applications could benefit from the quick separation times to be better able to detect small amounts of blood borne bacteria or virus.

In conclusion, the research presented here demonstrates the broad size range that current DC-iGDEP technology can separate, isolate, and concentrate. The polystyrene particle sizes used (20, 200 nm, and 1 μm) represent the sizes of several bioanalytes of interest: animal cells, bacteria, and viruses. Here DC-iGDEP demonstrated its ability to isolate and concentrate each of the sizes individually as well as co-capturing 1 μm and 200 nm particles simultaneously and reproducibly. Moreover, this capture was quick (few seconds to a few minutes) and reversible, opening up the possibilities for further analysis. The method has also shown its ability to resolve 20 nm particles, which lies toward the lower size limit of separation due to the Brownian motion. Finally, the enrichment factor found for 200 nm particles experimentally was 10^3 and could be expected to be as high as 10^6 in systems that are not overloaded with respect to particles. Combining the size range covered with the high levels of enrichment DC-iGDEP shows promise for future applications in separation and concentration of bioanalytes found in low levels such as bacteria and viruses in blood.

This research was financially supported in part through the Department of State Fulbright Fellowship and the Department of Education Foreign Language and Area Studies Fellowship (FLAS) as well as NIH grants 2RO1EB004761-06 and R21EB010191-01A1.

The authors have declared no conflict of interest.

5 References

[1] Pohl, H. A., *Dielectrophoresis*, Cambridge University Press, Cambridge 1978.

[2] Alper, J., *Anal. Chem.* 2008, *80*, 2285.

[3] Borgatti, M., Bianchi, N., Mancini, I., Feriotto, G., Gambari, R., *Int. J. Mol. Med.* 2008, *21*, 3–12.

[4] Pysher, M. D., Hayes, M. A., *Anal. Chem.* 2007, *79*, 4552–4557.

[5] Pohl, H. A., *J. Appl. Phys.* 1952, *22*, 869–871.

[6] Kovarik, M. L., Jacobson, S. C., *Anal. Chem.* 2008, *80*, 657–664.

[7] Cheng, I., Chang, H., Hou, D., Chang, H., *Biomicrofluidics* 2007, *1*, 021503.

[8] de la Rosa, C., Prakash, R., Tilley, P. A., Fox, J. D., Kaler, K. V. I. S., *Proceedings of the 29th Annual International Conference of the IEEE EMBS*, 2007, pp. 6302–6305.

[9] de la Rosa, C., Tilley, P. A., Fox, J. D., Kaler, K. V. I. S., *IEEE Trans. Biomed. Eng.* 2008, *55*, 2426–2432.

[10] Beck, J. D., Shang, L., Li, B., Marcus, M. S., Hamers, R. J., *Anal. Chem.* 2008, *80*, 3757–3761.

[11] Park, S., Beskok, A., *Anal. Chem.* 2008, *80*, 2832–2841.

[12] Varshney, M., Li, Y., *Talanta* 2008, *74*, 518–525.

[13] Docoslis, A., Tercero Espinoza, L. A., Zhang, B., Cheng, L., Israel, B. A., Alexandridis, P., Abbott, N. L., *Langmuir* 2007, *23*, 3840–3848.

[14] Park, K., Akin, D., Bashir, R., *Biomed. Microdev.* 2007, *9*, 877–883.

[15] Hubner, Y., Hoettges, K. F., McDonnell, M. B., Carter, M. J., Hughes, M. P., *Int. J. Nanomed.* 2007, *2*, 427–431.

[16] Meighan, M. M., Staton, S. J. R., Hayes, M. A., *Electrophoresis* 2009, *30*, 852–865.

[17] Cummings, E. B., Singh, A. K., *Anal. Chem.* 2003, *75*, 4724–4731.

[18] Lapizco-Encinas, B. H., Davalos, R. V., Simmons, B. A., Cummings, E. B., Fintschenko, Y., *J. Microbiol. Methods* 2005, *62*, 317–326.

[19] Gallo-Villanueva, R. C., Rodrỳguez-Lopez, C. E., Dıaz-de-la-Garza, R. I., Reyes-Betanzo, C., Lapizco-Encinas, B. H., *Electrophoresis* 2009, *30*, 4195–4205.

[20] Martinez-Lopez, J. I., Moncada-Hernandez, H., Baylon-Cardiel, J. L., Martinez-Chapa, S. O., Rito-Palomares, M., Lapizco-Encinas, B. H., *Anal. Bioanal. Chem.* 2009, *394*, 293–302.

[21] Calander, N., *Anal. Chem.* 2009, *81*, 8347–8353.

[22] Hindson, B. J., Gutierrez, D. M., Ness, K. D., Makarewicz, A. J., Metz, T. R., Setlur, U. S., Benett, W. B., Loge, J. M., Colston, J., Bill, W., Francis, P. S., Barnett, N. W., Dzenitis, J. M., *Analyst* 2008, *133*, 248–255.

[23] Clarke, R. W., Piper, J. D., Ying, L., Klenerman, D., *Phys. Rev. Lett.* 2007, *98*, 198102(198101–198104).

[24] Chen, K. P., Pacheco, J. R., Hayes, M. A., Staton, S. J. R., *Electrophoresis* 2009, *30*, 1441–1448.

[25] Mack, C., *Fundamental Principles of Optical Lithography: The Science of Microfabrication*, Wiley, Hoboken 2008.

[26] Haubert, K., Drier, T., Beebe, D., *Lab Chip* 2006, *6*, 1548–1549.

[27] Matthews, C. K., Ahern, K. G., Holde, K. E. V., *Biochemistry*, Benjamin-Cummings Company, Boston 1999.

[28] Ortega, Y. R. (Ed.), *Foodborne Parasites*, Springer, New York 2006.

[29] Medem, G., Teunis, P., Blokker, M., Deere, D., Davison, A., Charles, P., Loret, J.-F., World Health Organization 2006, p. 138.

[30] Ackermann, H.-W., Berthiaume, L., *Atlas of Virus Diagrams*, CRC Press, Boca Raton 1995.

[31] Palmer, E. L., Martin, M. L., *An Atlas of Mammalian Viruses*, CRC Press, Boca Raton 1982.

[32] Levy, J. A., *HIV and the Pathogenesis of AIDS*, ASM Press, Washington, DC 2007.

[33] Skoog, D. A., Holler, F. J., Nieman, T. A., *Principles of Instrumental Analysis*, Harcourt Brace College Publishers, Philadelphia 1998.

[34] Gupta, S., Alargova, R. G., Kilpatrick, P. K., Velev, O. D., *Soft Matter* 2008, *4*, 726–730.

[35] Cummings, E. B., Griffiths, S. K., Nilson, R. H., Paul, P. H., *Anal. Chem.* 2000, *72*, 2526–2532.

